Received: 31 March 2022 | Revised: 23 November 2022 | Accepted: 8 December 2022 | Published on: 26 December 2022

DOI: 10.1002/mrm.29565

RESEARCH ARTICLE

Magnetic Resonance in Medicine

Post-acquisition water-signal removal in 3D water-unsuppressed ^{1}H-MR spectroscopic imaging of the prostate

Angeliki Stamatelatou[1] | **Diana M. Sima**[2] | **Sabine van Huffel**[3] | **Jack J. A. van Asten**[1] | **Arend Heerschap**[1] | **Tom W. J. Scheenen**[1]

[1]Department of Medical Imaging (766), Radboud University Medical Center Nijmegen, Nijmegen, The Netherlands

[2]icometrix, R&D, Leuven, Belgium

[3]STADIUS Center for Dynamical Systems, Signal Processing and Data Analytics, Department of Electrical Engineering (ESAT), Leuven, Belgium

Correspondence
Angeliki Stamatelatou, Department of Medical Imaging (766), Radboud University Medical Center Nijmegen, Geert Grooteplein 10, PO Box 9101, 6500 HB Nijmegen, The Netherlands.
Email: angeliki.stamatelatou@radboudumc.nl

Funding information
European Union's; Marie Sklodowska-Curie, Grant/Award Number: 813120; Flemish Government

Purpose: To develop a robust processing procedure of raw signals from water-unsuppressed MRSI of the prostate for the mapping of absolute tissue concentrations of metabolites.

Methods: Water-unsuppressed 3D MRSI data were acquired from a phantom, from healthy volunteers, and a patient with prostate cancer. Signal processing included sequential computation of the modulus of the FID to remove water sidebands, a Hilbert transformation, and k-space Hamming filtering. For the removal of the water signal, we compared Löwner tensor-based blind source separation (BSS) and Hankel Lanczos singular value decomposition techniques. Absolute metabolite levels were quantified with LCModel and the results were statistically analyzed to compare the water removal methods and conventional water-suppressed MRSI.

Results: The post-processing algorithms successfully removed the water signal and its sidebands without affecting metabolite signals. The best water removal performance was achieved by Löwner tensor-based BSS. Absolute tissue concentrations of citrate in the peripheral zone derived from water-suppressed and unsuppressed ^{1}H MRSI were the same and as expected from the known physiology of the healthy prostate. Maps for citrate and choline from water-unsuppressed 3D ^{1}H-MRSI of the prostate showed expected spatial variations in metabolite levels.

Conclusion: We developed a robust relatively simple post-processing method of water-unsuppressed MRSI of the prostate to remove the water signal. Absolute quantification using the water signal, originating from the same location as the metabolite signals, avoids the acquisition of additional reference data.

KEYWORDS

^{1}H MRSI, 3 T, metabolite concentrations, post-processing, prostate, water removal, water-unsuppressed

1 | INTRODUCTION

Worldwide, prostate cancer is the second most common cancer and the fifth leading cause of cancer death among men.[1] Multi-parametric MR imaging (mpMRI) is increasingly used in the detection, localization, and grading of the disease.[2] MpMRI consists of T_2-weighted MRI to visualize anatomy and of functional MR techniques, such as DWI,[3] DCE-MRI,[4] and MRSI.[5] The Prostate Imaging Reporting and Data System (PIRADS)[6–8] is used in clinical practice to read and report mpMRI exams, but does not include MRSI in the latest version because of insufficient clinical robustness and practicality of MRSI procedures.[5] However, recent MRSI acquisition methods demonstrate substantially improved performances[5,9] and therefore, may enhance current mpMRI as this still suffers from low specificity and inter-reader reproducibility.[10,11]

Proton MR spectra of the prostate contain signals from citrate (Cit), choline-containing compounds (Cho), (phospho-) Cr, and polyamines (PA) (i.e., spermine [Spm]). In cancer tissue, Cit signals are reduced and those of Cho are increased compared to normal prostate tissue. Ratios of metabolite signals, such as (Cho + PA + Cr)/Cit or Cho/Cr are used for the identification and characterization of prostate cancer.[12,13] Because the metabolite signals may be corrupted by large signals of water and lipids, these are suppressed with water and lipid dual-frequency selective refocusing pulses combined with strong spoiler gradients.[14] Although quite robust, the suppression performance of these pulses depends on B_0 homogeneity in and around the prostate. Moreover, these pulses may suppress signals with a chemical shift close to that of water and could result in magnetization transfer effects on metabolite signals, which can cause errors in their quantification.[15,16]

Recently, we demonstrated that water-unsuppressed 3D ^{1}H MRSI of the prostate is feasible and has advantages compared to water-suppressed MRSI.[17] For instance, the unsuppressed water signal is useful to correct for line shape artifacts and to estimate absolute tissue concentrations of metabolites. It also facilitates the accurate combination of signals from multiple elements of body array coils, which is a challenge in water-suppressed acquisitions with low SNR levels.[18,19] For these purposes, in single-voxel MRS a water signal is traditionally obtained by a separate MRS acquisition without water suppression.[20] However, in an MRSI exam, an extra water-unsuppressed acquisition may require too much additional time.

Therefore, an MRSI acquisition without water signal suppression is an attractive option, provided the metabolite signals of interest can robustly be recovered.[15,16,21,22] This may be challenging as localization gradient vibrations generate water sideband artifacts, which can overlap with metabolite signals.[16] A common way to remove these sidebands is by computing the modulus of the time-domain MRS signal.[15,16,23] Previously, we applied this approach to water-unsuppressed MRSI of the prostate and used wavelet transforms to extract the water signal and to reconstruct the baseline. Multiple corrections were applied on phase and frequency deviations and on eddy current artifacts, followed by metabolite signal fitting with the modeled water signal shape, altogether consisting of an extensive and complex MRSI data processing pipeline.[17]

The main aim of the current study is to replace this pipeline with a more efficient and simpler procedure, including alternative water-signal removals, modulus transformation to automatically align the phase and frequency of all signals, and spatial filtering applied after these alignments to enhance SNR.[21] For the water-signal removal, we investigated Hankel Lanczos singular value decomposition (HLSVD)[24,25] and Löwner tensor-based blind source separation (BSS).[22] The performance of these algorithms was compared with each other and with that of conventional water suppression in a phantom and volunteers. Finally, we used the extracted water signal, for absolute metabolite quantification from MRSI's of the prostate recorded with and without water-signal suppression to investigate any effect of this suppression and to reconstruct metabolite maps.

2 | METHODS

2.1 | Phantom and subjects

In vitro studies were performed with a spherical glass phantom, consisting of a solution mimicking prostatic fluid, containing 90 mM Cit, 18 mM Spm, 6 mM myo-inositol, 15 g/L bovine serum albumine, and cations at pH 7.1.[26] Furthermore, we examined five healthy volunteers (27–55 years, mean age, 47 years) and one patient with prostate cancer (69 years) before prostatectomy, with two tumor lesions in the prostate with Gleason scores 3 + 4. Ethical approval for these measurements was obtained by the local ethics committee and all volunteers and the patient gave written informed consent for participation in the study.

2.2 | MR data acquisition

A 3 T MR system (MAGNETOM Prisma-Fit, Siemens Healthcare, Erlangen, Germany) was used with an external 16-channel body phased-array coil for signal reception in the phantom study and in the volunteers. In the patient examination, an additional endorectal coil (MEDRAD, Pittsburgh, PA) for signal reception was used.

Three-dimensional MRSI data were acquired with a semi-LASER (localized by adiabatic selective refocusing) pulse sequence in which a 3D volume of interest (VOI) is selected with conventional slice selective excitation and two pairs of adiabatic refocusing pulses.[27] In the phantom study, the TR was 1250 ms and the TE was 88 ms (optimized for Cit shape).[27] Spectra were sampled with 2048 spectral points at a spectral bandwidth of 3200 Hz (26 ppm). The spatial FOV of $64\,mm^3 \times 64\,mm^3 \times 64\,mm^3$ was covered with an $7 \times 7 \times 7$ elliptically sampled k-space matrix, acquired with 1 average. After post-processing with a Hamming filter (see below) the true voxel size can be approximated by a sphere with a volume of 2.2 cm^3. Water and lipid signal suppression was performed with a double Mescher-Garwood (MEGA) module of water and lipid-selective refocusing pulses combined with coherence crushing by strong spoiler gradients.[14] Two MRSI datasets were acquired: one with the full MEGA modules and one with MEGA pulses only refocusing and suppressing lipid signals (the water-unsuppressed dataset). Signals of the different body array coil elements were combined in a weighted and phase sensitive way using a complex fit to the first points of the sLASER spin echo top for each coil element.

The subjects were examined with the same acquisition protocol, but with a TR of 950 ms in the volunteers and 1930 ms in the patient. In the volunteers, the FOV of $80\,mm^3 \times 80\,mm^3 \times 64\,mm^3$ was covered with a $7 \times 7 \times 7$ k-space matrix, acquired with 4 Hamming-weighted averages. After post-processing the true voxel size can be approximated by a sphere with a volume of 3.6 cm^3. The total acquisition time was 10 min and 2 s. In the patient, because of examination time constraints, we only acquired a dataset without suppression of the water signal (MEGA lipid suppression only), with a spectral bandwidth of 2400 Hz (19.5 ppm), the FOV of $64\,mm^3 \times 80\,mm^3 \times 64\,mm^3$ was covered with a $9 \times 11 \times 9$ k-space matrix, acquired with 3 Hamming-weighted averages. After post-processing the true voxel size can be approximated by a sphere with a volume of 1.1 cm^3. The total acquisition time was 12 min and 30 s. In the patient study with endorectal coil, the MR system lowers the allowed RF power deposition by 50%, so a longer TR was necessary to stay within specific absorption rate limits.

For all the MRSI datasets, T_2-weighted MR images were acquired for anatomical guidance.

2.3 | MRSI data processing

Data processing modules were programmed in MATLAB (MATLAB R2019b, The MathWorks, Natick, MA) with some format conversions to allow visualization on existing image viewers (Siemens Syngo software). The processing pipeline is illustrated in Figure 1. For the statistical analysis Origin (Origin 8.5) was used.

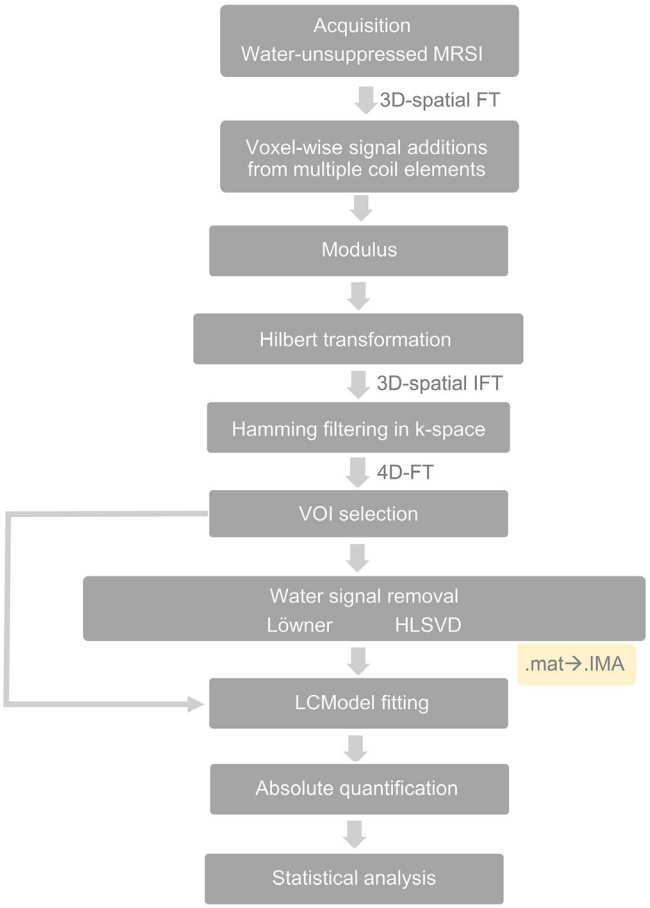

FIGURE 1 Flow diagram representing the processing pipeline of water-signal unsuppressed 3D ^{1}H MRSI.
IMA, single-precision DICOM MRSI files obtained with Siemens MR systems.mat, MATLAB files; VOI, volume of interest.

Data processing started with zero filling of a 3D MRSI k-space data set to a $16 \times 16 \times 16$ matrix and Fourier transformation of the spatial k-space dimensions. Next, acoustic sideband artifacts in the MR spectra were eliminated by computing the modulus signal of the FIDs in all voxels, an operation that also corrects the phase and aligns the frequency of all signals.[21,23]

From the modulus signals, a Hilbert transformation was performed in the time domain to create again a complex signal. The Hilbert transform is based on the Kramers-Kroning relations.[28] The Hilbert transform for a real input signal returns a complex result of the same length, where the real part of the output is the original real data and the imaginary part is the actual Hilbert transform, so the real signal with a 90° phase shift. Within the procedure zero filling (before the Hilbert transformation) and data truncation (after the transformation) in the time domain is applied to avoid the discontinuity

in the lineshape of the water signal. After modulus and Hilbert transformation of the FIDs, an inverse Fourier transformation (iFT) of the three spatial dimensions was performed to allow the application of a 3D k-space Hamming filter to the data. As the modulus operation applied before k-space filtering aligned signal frequencies, line broadening due to the convolution of signals with slightly different frequencies by the k-space Hamming filter was avoided; this alleviated potential SNR loss induced by the modulus step.[21]

The next step was the water-signal removal. This was only done for voxels within the VOI to avoid long computation times. The Löwner tensor-based BSS[24,25,29] and HLSVD[24,25,29] algorithms were investigated as computational techniques for water-signal removal. The Löwner BSS method is a tensor-based algorithm that is used to remove the water signal simultaneously from all voxels in the MRSI grid. The water signal is modeled under the assumption that neighboring voxels in the MRSI grid share common signal components (sources). Therefore, the estimation of sources that model water and their corresponding abundances can be formulated as a BSS problem to estimate the individual metabolite sources. The model order (i.e., the total number of estimated sources to model the whole grid) was assumed to be known a priori[22] and was chosen to be 100 for both Löwner and HLSVD algorithms to make sure all the variations in damping across signals in the MRSI grid were sufficiently captured. The Löwner tensor was constructed using the spectroscopic range from 1.2 to 5.2 ppm, which contains the region with metabolite signals (1.2–4.2 ppm), and that with the water signal (4.2–5.2 ppm).[5] The HLSVD method removes water in one voxel at a time and does not exploit the shared information present among the voxels in the MRSI grid. Using a truncated signal subspace decomposition of a priori known model order, the water signal in 4.2–5.2 ppm was estimated as a sum of complex damped exponentials and subsequently removed from the measured signal.[14,30]

Subsequently, the processed MR spectra were fitted and quantified with LCModel software (version 6.3–1 L).[27,31] The basis-set for the LCModel fitting was simulated with NMR-Sim (Bruker BioSpin, Rheinstetten, Germany). To estimate absolute tissue concentrations of metabolites the water signal was used as a scaling reference, for which the water-unsuppressed MR spectra were deployed before water removal from the same MRSI acquisition as used for the metabolite MR spectra. For the LCModel fitting, a basis set was generated with Lorentzian-type proton signals for Cit, Cho, Spm, and Cr, taking into account the exact timings of the sLASER pulse sequence.

2.4 | Tissue concentrations of metabolites

For absolute quantification of metabolite tissue concentrations in the prostate, the metabolite values from the LCModel fits (*LCMoutput(met)*, Eq. [1]) were calculated using a 1 ppm broad water signal area as a concentration reference, extracted from the same spectra and corrected by the T_1 and T_2 relaxation times for water ($T_{1,H2O}$, $T_{2,H2O}$) and metabolites ($T_{1,met}$, $T_{2,met}$), according to Eq. [1 with values as reported in literature.[5] For Cit at 3 T, the T_1 and T_2 values were 0.47 ± 0.14 s and 0.17 ± 0.05 s, respectively. For Cho, the T_1 and T_2 values were 1.1 ± 0.4 s and 0.22 ± 0.09 s, respectively. For water in the peripheral zone of the prostate, the T_1 and T_2 were 1.60 ± 0.04 s and 0.14 ± 0.03 s, respectively.[32–34] Finally, the tissue metabolite concentrations were calculated taking the tissue water concentration as reference (*wconc*, Eq.[1]), assuming a tissue water content in the prostate of 39.4 mM/g wet weight[35] and a prostate tissue density of 1.02 kg/L[36,37]

$$[Metabolite] = LCMoutput(\text{met}) \times \frac{\left[1 - e^{\left(-\frac{TR}{T_{1,H2O}}\right)}\right]\left[e^{\left(-\frac{TE}{T_{2,H2O}}\right)}\right]}{\left[1 - e^{\left(-\frac{TR}{T_{1,met}}\right)}\right]\left[e^{\left(-\frac{TE}{T_{2,met}}\right)}\right]} wconc \quad (1)$$

2.5 | Comparison between water removal algorithms and conventional water suppression, and statistical analysis

To evaluate the effect of the water removal methods on the quantification of metabolites of interest in the phantom, a one-way repeated measures analysis of variance (ANOVA) was applied to Cit concentrations as obtained from the LCModel output. No attempt was made to compare absolute concentrations as the relaxation time correction factors, required for this determination, are the same for water suppressed and unsuppressed MRSI data and therefore, are irrelevant to compare Cit levels.

To compare the water removal algorithms and the conventional water suppression in volunteers we determined, first the efficiency of the water-signal removal, second, the failure rate of techniques to sufficiently suppress/remove the water signal, and third the effect of the techniques on the absolute quantification of Cit.

To assess the efficiency of the methods to remove the water signal in MR spectra of the healthy volunteers, we compared the ratios of the variance of water

signal residual (4.2–5.2 ppm) to the variance in a spectral area with only noise (10.8–12.0 ppm). Next, the outliers of the variance ratio were identified, according to the 1.5 interquartile range (IQR) rule; the number of outliers was considered as an indication of failure of the methodologies used to suppress the water signal. Finally, to explore a possible effect of the water removal methodologies on the quantification of metabolites of interest, a one-way repeated-measure ANOVA was performed on the absolute metabolite concentrations. For this analysis, values from non-overlapping spatially independent voxels were selected, originating from the peripheral zone of the prostate, with a Cramer-Rao lower bound of fitted metabolite values <20%, which were not judged as outliers in the previous comparison.

3 | RESULTS

Proton MR spectra from the prostate of a healthy volunteer, obtained with a sLASER MRSI sequence without water suppression, showed dominating large water signals as well as metabolite signals (Figure 2). In the water unsuppressed spectra, anti-symmetrically around the center of the water peak, sideband artifacts are present. These water-signal sidebands were most clearly visible in water-unsuppressed MR spectra of the phantom (Figure 3A), but could also be detected in MR spectra obtained in vivo (Figure 4). The sidebands were effectively removed with the modulus step (Figure 3A). Moreover, this step aligned the water signal from all voxels at one frequency, which was set to 4.7 ppm as a reference chemical shift (Figure 3B).

After the modulus operation (Figure S1D), Hilbert transformation (Figure S1E), 3D spatial iFT, spatial smoothing by Hamming filtering of 3D k-space (Figure S1F), and a 4D FT, the water removal algorithms were applied. As shown for an MR spectrum of a voxel from 3D MRSI measurements of a volunteer the water signal was successfully suppressed in MRSI with water-suppression pulses and equally successfully removed by the Löwner and HLSVD algorithms from the

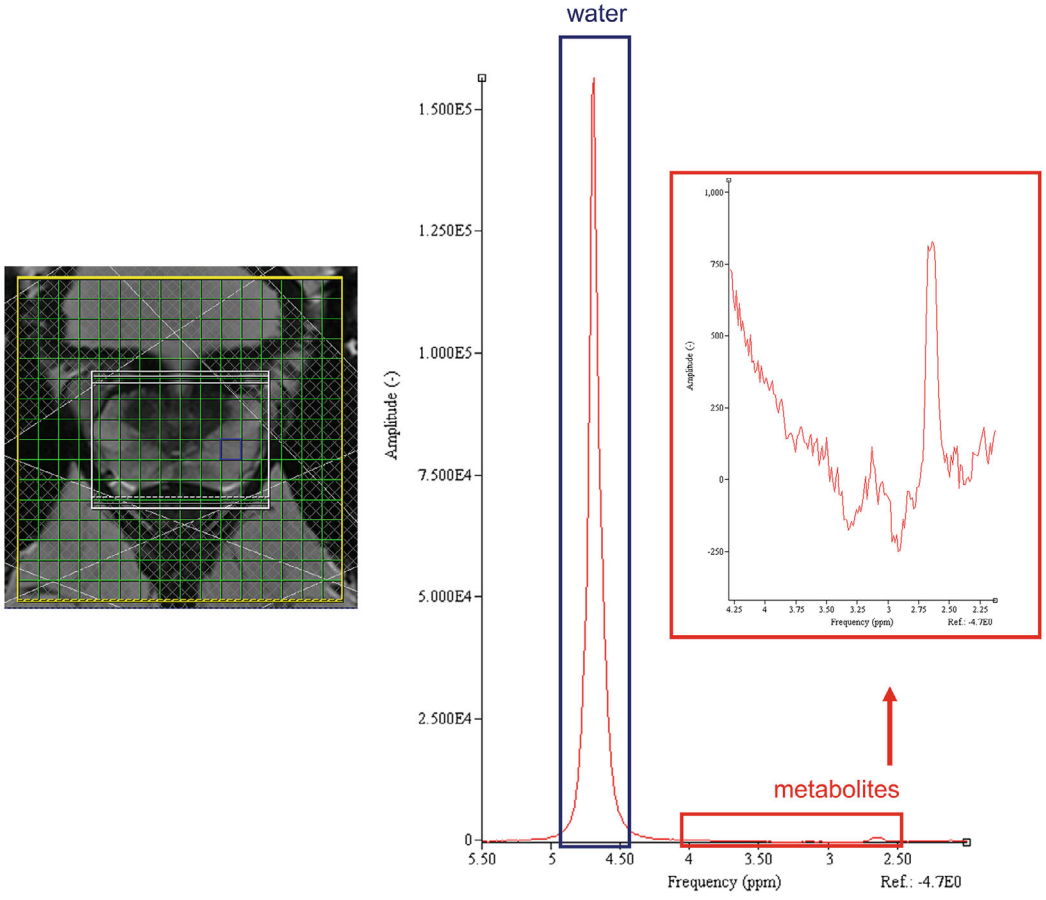

FIGURE 2 Water-signal unsuppressed 3D ^{1}H-MRSI of the prostate of a 46-year-old healthy volunteer. Left: Transversal T_2 weighted MRI with the MRSI grid. The VOI embedding the prostate is indicated by the white box. Middle: MR spectrum from a voxel of this VOI. The blue box highlights the water peak. The area with signals of metabolites of interest is indicated with a red box. Upper right: Enlargement of part of the MR spectrum showing metabolite signals (in the red box). The metabolite peaks are orders of magnitude smaller than that of water.

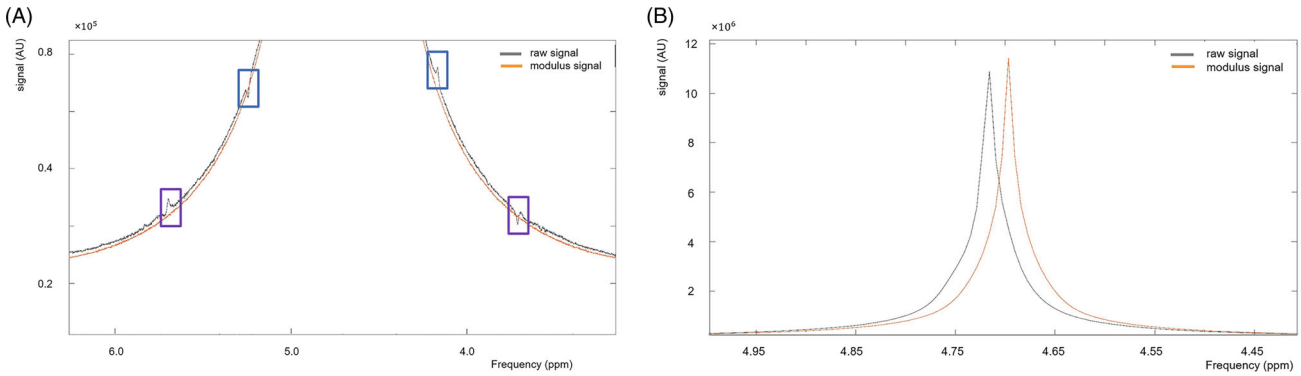

FIGURE 3 Effect of modulus operation on water signal of a phantom. Water signal of a phantom, filled with prostatic fluid mimic, acquired with a semi-LASER (sLASER) water-signal unsuppressed MRSI pulse sequence. The effect of the modulus operation on the sideband artifacts. The water signal before (gray) and after the modulus step (orange). Sideband artifacts are symmetrically present on both sides of the water peak (blue and purple boxes) in the raw signal (gray). After the modulus step, these artifacts are eliminated. The effect of modulus operation on the frequency shift artifacts. This water signal is shifted because of the modulus operation. It is then assigned a chemical shift of 4.7 ppm (orange). As this happens to all water signals in the VOI they become aligned.

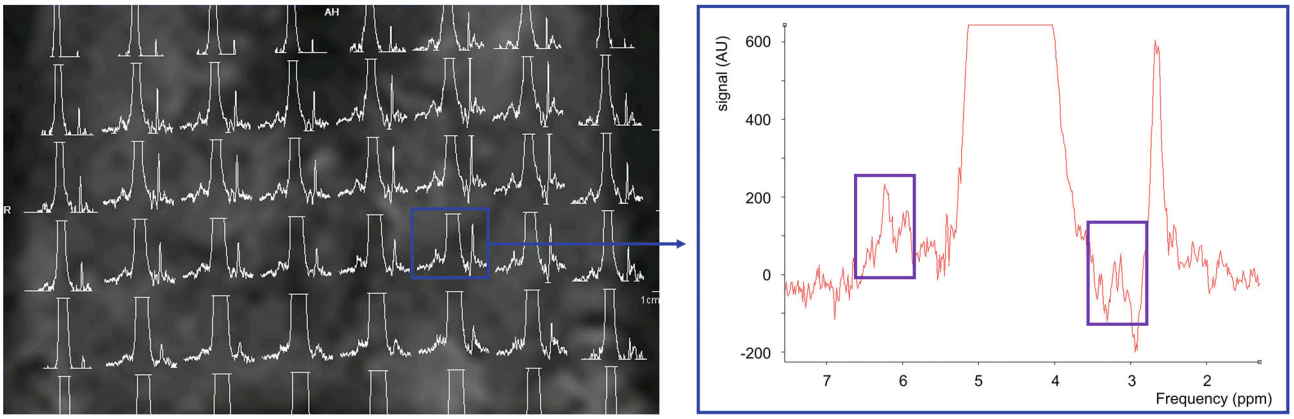

FIGURE 4 Water sidebands in in vivo MR spectra. Spectral map and enlarged spectrum of the water signal and the metabolites of interest region from a healthy volunteer, illustrating the presence of water sidebands around 6.1 and 3.3 ppm throughout this partition of the prostate. The sideband artifacts are symmetrically present on both sides of the water peak (purple boxes) in the raw signal, interfering with the region of the metabolites of interest (2.3–3.6 ppm), which can cause inaccurate assessments of the metabolites of interest.

water-unsuppressed MRSI (Figure 5). In this example, the conventional water-signal suppression method and the two algorithms all effectively have removed the water signal to or below the noise level, leaving a high SNR signal for Cit at 2.6 ppm and other metabolites signals at about 3–3.5 ppm (i.e., Cho, Cr, and Spm).

3.1 | Three dimensional MRSI of the phantom with a prostatic metabolite solution

To examine if the post-acquisition water removal interferes with the quantification of metabolite signals, we assessed the Cit levels in the phantom after the removal of the water signal in water-unsuppressed MRSI by the Löwner and HLSVD methods and in water-suppressed MRSI. The Cit levels were evaluated in 42 voxels within the phantom. No corrections for T_1 and T_2 relaxation times were made. The water-signal removal algorithms and water-signal suppression did not differ significantly in Cit levels, according to an ANOVA statistical analysis ($\alpha > 0.05$). An example of the LCModel fit of an MR spectrum from the MRSI obtained of the phantom is presented as supporting information in Figure S2.

3.2 | In vivo MRSI in healthy volunteers

To assess the efficiency of the water-signal removal we compared the ratio of signal variance in the water range (4.2–5.2 ppm) to the variance in the noise range

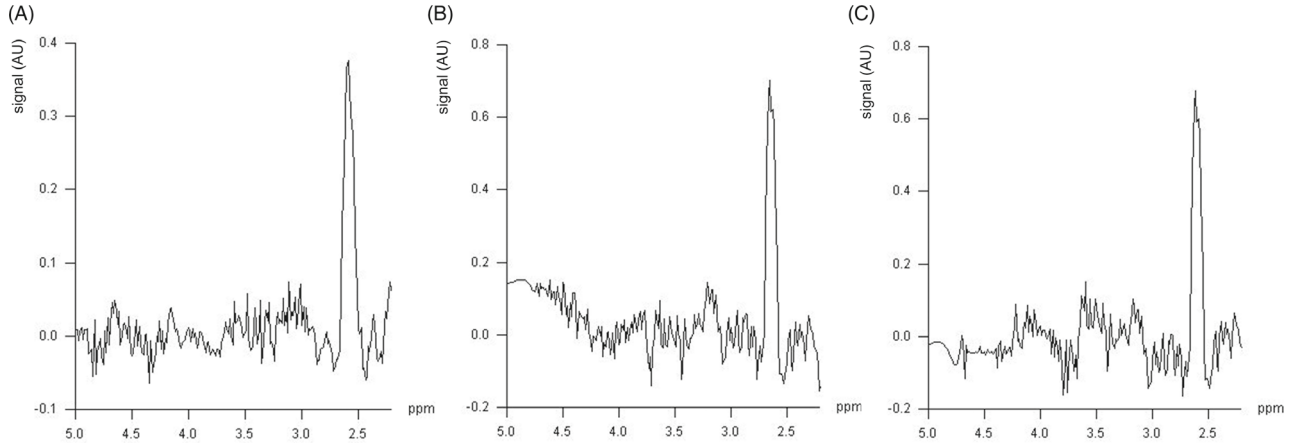

FIGURE 5 Water signal removal. MR spectra from the same voxel of 3D MRSI data of a healthy volunteer in the chemical shift range 2.0–5.0 ppm. (A) An MR spectrum obtained with water signal suppressed MRSI. MR spectra with water-signal unsuppressed MRSI and water signal removal using. (B) The Löwner BSS algorithm. (C) The HLSVD algorithm. BSS, blind source separation; HLSVD, Hankel Lanczos singular value decomposition

(10.8–12.0 ppm). In total, 306 spectroscopic ratios were assessed from all the voxels in the volumes of interest of the five volunteers. The mean values found were 0.95 ± 0.44 for Löwner BSS, 7.86 ± 14.20 for HLSVD, and 3.46 ± 1.95 for the conventional water suppressed acquisition. Löwner BSS provided the best suppression of the water peak with respect to the noise level. Whereas in some spectra the water signal is removed below the noise level, indicating that some noise was modeled and removed with the technique, there are also areas in which some small residuals remain. On average, the water signal is removed just below the noise level with Löwner BSS, whereas HLSVD and conventional water suppression during acquisition left some residual water signal.

If water removal fails, metabolite quantification might be hampered. The failure rate of the techniques to sufficiently suppress/remove the water signal was examined by the outliers of the variance ratio. In Figure 6, the range of the values of water residual variance to the noise variance is presented for all the voxels ($N = 306$) in the volumes of interest from the five volunteers. After the application of Löwner BSS no outliers were identified, whereas applying HLSVD resulted in 40 outliers of 306 spectra, and in the conventional water suppression, 10 outliers were identified of 306 spectra. Therefore, Löwner BSS performed the best in removing the water signal, because the range of the variance ratio is narrow and without outliers.

The effect of the water suppression algorithms on metabolite quantification was investigated in the spectroscopic range from 1.2 to 3.8 ppm (Table 1). We selected 40 spatially independent voxels in the peripheral zones of the five volunteers for this analysis.

A repeated-measures ANOVA statistical analysis was performed to assess the effect of the water-signal

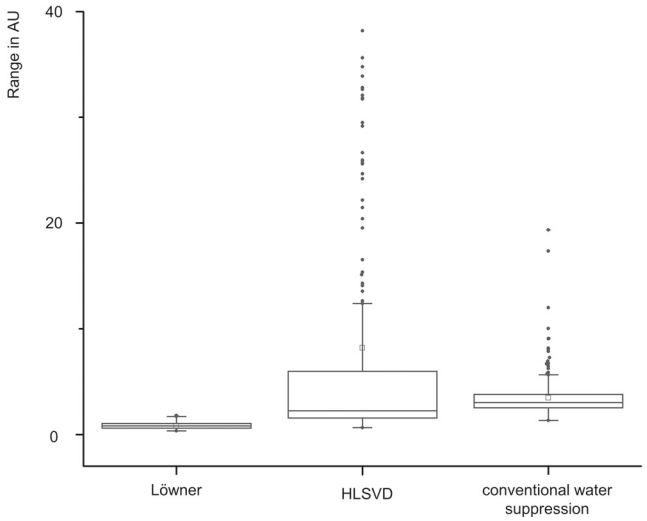

FIGURE 6 Water signal/noise variance ratio range for water signal suppression/removal. The range of the values of variance in the area of water to the variance in the area of noise is presented for Löwner BSS and HLSVD water signal removal and conventional water suppression. The results from 306 voxels located in the volume of interest from the five volunteers are presented in the range up to 40 AU. In the case of HLSVD 16 additional outliers are presented above this range. The outliers (i.e., the voxels where the water signal removal/suppression failed) are identified (points outside of the box) according to the 1.5 interquartile range (IQR) rule. The mean values of the variance ratios are presented as a square symbol. BSS, blind source separation; HLSVD, Hankel Lanczos singular value decomposition

removal/suppression method on the absolute Cit levels in 40 selected voxels from the prostate of five volunteers. The absolute tissue concentration of Cit did not differ significantly between Löwner BSS, HLSVD water-signal

TABLE 1 Statistical analysis of absolute tissue concentrations of Cit calculated from MRSI data obtained of the prostate of healthy volunteers A. Mean absolute Cit tissue concentrations as obtained by water-signal unsuppressed MRSI involving the water signal removal methods (Löwner, HLSVD) and by water signal suppressed MRSI B. Absolute Cit tissue concentration in the peripheral zone of the prostate reported by Basharat et al.[41] C. ANOVA statistical analysis comparing the water signal removal and suppression methods ($\alpha = 0.05$) for the absolute Cit concentrations

A	**Cit mean value (mM)**	**SD (%)**	***p*-value**
Lowner	41.21	7.9	
HLSVD	41.16	8.3	
WS	42.64	7.5	
B	**Cit (mM)**	**SD**	
Literature peripheral zone	64	±22	
C	**Cit mean difference**	**Significant difference**	
Lowner vs HLSVD	0.04	No	1.0
HLSVD vs WS	−1.49	No	0.08
Lowner vs WS	−1.45	No	0.09

Note: $N = 40$ voxels from the five healthy volunteers; WS = water signal suppressed acquisition.

removal, and the conventional water suppression ($\alpha > 0.05$) (Table 1).

3.3 | Metabolite maps of the prostate of a healthy volunteer and prostate cancer patient

The absolute tissue concentrations of Cit in the prostate of a healthy volunteer, obtained from a water-signal unsuppressed MRSI and water-signal removal with Löwner BSS, were used to create metabolite maps of multiple slices as an overlay on the T_2-weighted images for anatomical reference information (Figure 7). In the peripheral zone of the prostate, Cit levels up to 50.0 mM were observed, much higher than in the central gland, with Cit levels down to about 20.0 mM.

The Löwner BSS water-signal removal method was also applied to a water-unsuppressed 3D MRSI data set of the prostate of a patient. Examples of LCModel fits of MR spectra from a healthy voxel and from a cancerous voxel are presented in Figures S3 and S4, respectively.

After absolute quantification of the metabolites with signals visible in the MR spectra, maps of Cit and Cho were created for two slices of the patient's prostate (Figure 8). Areas with relatively low Cit (12.0 mM) and high Cho levels (up to 5.0 mM) were observed in the peripheral zone (Figure 8A,B), which corresponded to the presence of cancerous tissue, according to the histopathology report of the prostate after prostatectomy (Figure 8D).

4 | DISCUSSION

In this study, we successfully developed and applied a method to process water-signal unsuppressed MRSI data of the prostate. The modulus of the FID was selected to eliminate the water-signal sidebands as well as phase and frequency differences between the spectroscopic signals. By performing these alignments before applying a Hamming function to the MRSI data, any line broadening caused by this spatial filter was avoided. For the removal of the water-signal, we found that a Löwner BSS algorithm performed better than an HLSVD algorithm and the conventional water suppression. Absolute quantification of metabolites was achieved by LCModel signal fitting, using the unsuppressed water-signal as a reference. Altogether, the final post-processing algorithm was substantially simpler, shorter, and more efficient than the post-processing pipeline used for the first water-unsuppressed 3D MRSI of the prostate.[17]

The standard in ^{1}H MRSI of the prostate is to suppress the strong signals of water and lipids, which is most often done with dual-frequency selective refocusing pulses in combination with strong spoiler gradients.[38] This generally works successfully over large parts of the prostate, but may come with problems such as large residual water and lipid signals, overlapping metabolite

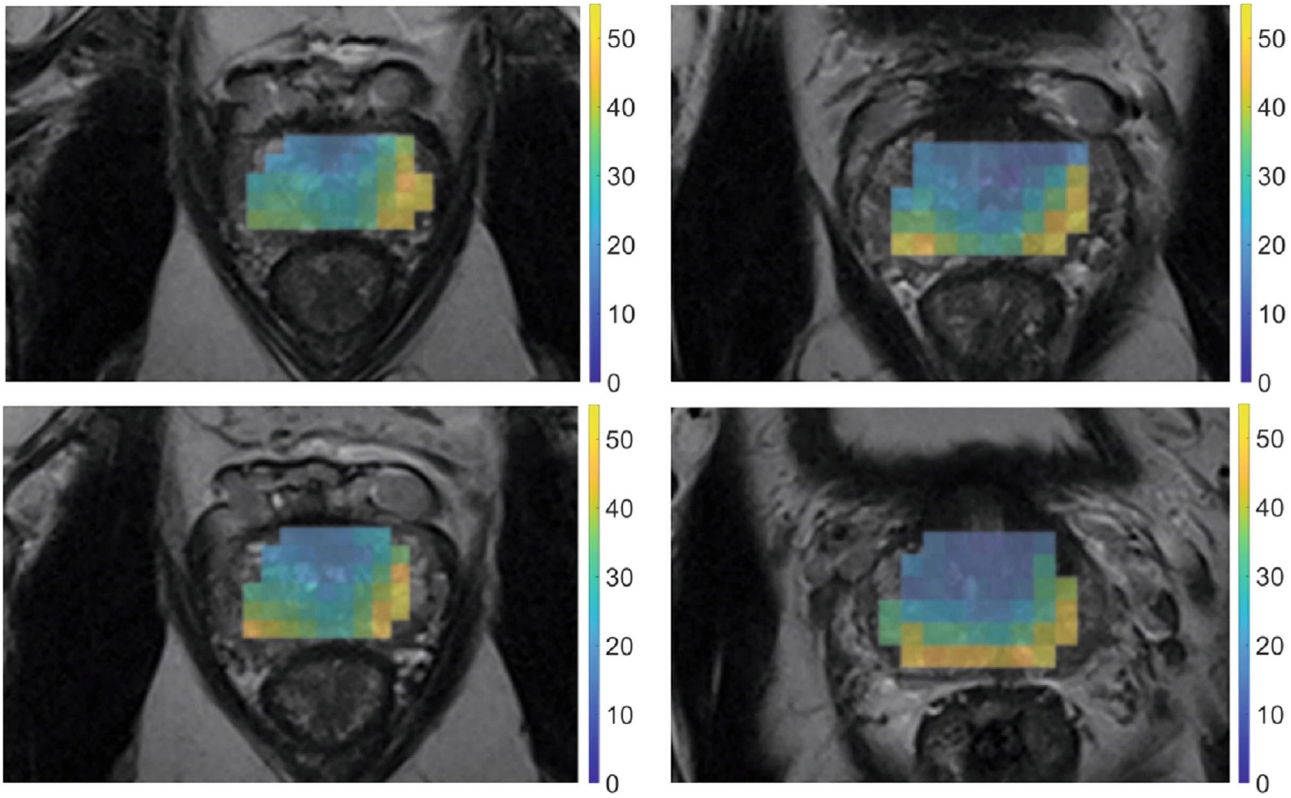

FIGURE 7 Transversal maps of absolute tissue concentrations of Cit (mM) in the prostate of a healthy volunteer. Water removal was done after the acquisition of water-signal unsuppressed MRSI with the BSS Löwner algorithm. Cit maps are shown at four different positions, overlaid on the T_2-weighted images for anatomical reference information. Cit, citrate; BSS, blind source separation;

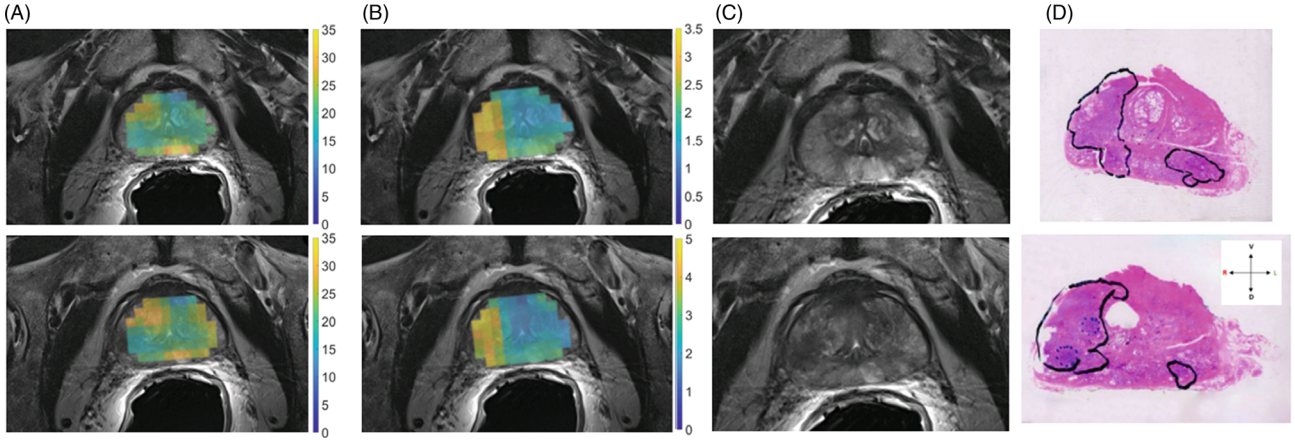

FIGURE 8 Metabolite maps of a patient with prostate cancer. (A) The metabolite maps of absolute tissue concentration of Cit in mM, in two axial slices. (B) The metabolite maps of absolute tissue concentration of Cho in mM, in the same two axial slices. (C) The corresponding anatomical T_{2w} images. (D) The histopathology results after prostatectomy are presented from approximately the same location as the axial slices. The two tumors in the peripheral zone of the prostate of this patient with Gleason scores 3 + 4 have relatively low Cit and high Cho levels. Cit, citrate

resonances, when B_0 inhomogeneities are present.[38] In contrast, not suppressing the water signal has several advantages, as this signal can be used as a reference, for instance for lineshape and frequency corrections and absolute metabolite quantification.[39] Using the water signal from the same scan has the inherent benefit of an exact co-localization of quantified metabolites with the water reference without the need for additional measurement

time. For these reasons, it is appealing to explore the possibilities of water-signal unsuppressed MRSI of the prostate.[17]

A major problem in water-signal unsuppressed ^{1}H MRSI is the water-signal sideband artifacts caused by vibrations of the localization gradients.[16] However, following previous work,[15,16,23] we could eliminate these artifacts by computing the modulus of the time-domain MRS signal. This transformation has the additional benefit that it automatically aligns the phase and the frequency of the spectroscopic signals. As modulus transformation induces symmetry of the spectrum around the water signal it comes with a theoretical SNR loss up to a factor of $\sqrt{2}$.[21] In practice, this SNR loss is limited as has been demonstrated in several ^{1}H MRSI brain studies, which is attributed to a different noise distribution and various corrections imposed by the modulus computation.[16,21,23] Moreover, to recover any SNR loss we applied spatial apodization by k-space Hamming filtering after the modulus process.[21] In this way, line broadening caused by this filtering, because of the addition of signals with different frequencies and phases, is avoided.

To remove the large water signal in water-unsuppressed MRSI we investigated the performance of HLSVD[24,25,40] and Löwner BSS[22] and compared these with results of conventional water-signal suppression during acquisition. In the phantom study, we showed that these post-acquisition water removal methods did not interfere with the quantification of the metabolites of interest. The water signal and the satellite peaks were sufficiently removed to end up with spectral shapes similar to the spectra acquired with water-signal suppression during the acquisition. The quantified amount of Cit did not differ significantly between the post-processing methods for water-signal removal and conventional water suppression.

In the in vivo MRSI study of the healthy volunteers, we evaluated three factors to identify the best performing water-signal removal or suppression: the efficiency of the water-signal removal, the failure rate to sufficiently suppress/remove the water signal, and the effect of the techniques on quantification of Cit. With both the lowest mean–variance ratio as well as the lowest number of outliers the Löwner tensor-based BSS method provided the highest efficiency of water-signal removal. Although HLSVD is the most widely used method for signal residual removal in post-processing,[40] as it is applied on a voxel-by-voxel basis and as it computes the water source components separately for each voxel, it does not exploit the information shared among the voxels in the MRSI grid. Hence, this algorithm can fail to remove the water signal completely because of noise or artifacts present in some voxels. Contrary to a voxel-by-voxel approach, the Löwner BSS method is applied simultaneously on the full MRSI grid to use a large number of sources that can be used, in various combinations, to model the water component in all voxels. The water signal in each voxel is then estimated as a linear combination of the sources with different voxel-specific weights, helping to prevent failures in water removal in single voxels.

Taken together the modules to process water-unsuppressed MRSI of the prostate, as developed in this study, are substantially more efficient and less complex than those initially applied to process water-unsuppressed MRSI of the prostate.[17] Although in the latter work multiple separate phase corrections and frequency alignments were performed, in the present work these corrections and alignments were automatically performed by the same single modulus transformation of the time-domain MRS signal that also was used to remove the water acoustic sidebands.[15,16,23] The initial post-processing also involved multiple eddy current corrections.[17] Although we have not performed these in the present work, it has been pointed out that the selection of the modulus inherently corrects for eddy current artifacts.[23] Additionally, in the previous study, the water signal and the spectroscopic baseline were extracted separately and combined to subtract from the original spectra data to obtain water signal-free and baseline corrected MR spectra. This lengthy procedure was replaced in our study by a single step applying a water-signal filter (Löwner-BSS). Furthermore, because the MRSI data of the prostate were recorded at a TE of 88 ms no specific baseline correction was deemed necessary as in earlier work it was observed that the spectroscopic contribution of macromolecules in MR spectra of the prostate acquired at a TE of 32 ms was already negligible.[41] Finally, to fit the metabolite signals we initially developed an algorithm applying the water-line shape as prior knowledge, whereas in the current study the commonly used LCModel software was used in which a basis set was constructed with Lorentzian shaped lines. This produced satisfactory results, but if needed the procedure could be improved by first converting the experimental shape of metabolite signals to Lorentzians by methods such as Quality using the water lineshape.[42]

Using the water signal from water-unsuppressed MRSI of the prostate of volunteers as an internal reference we determined the absolute tissue concentrations of Cit in the peripheral zone of these prostates. The values of about 41 mM are in the range of those previously reported for the normal peripheral zone in vivo[5,41] (i.e., from 27 mM to ~64 mM). No significant difference was found between the water removal in post-processing and the conventional water suppression methods. A difference between the water-signal suppressed and unsuppressed acquisitions

is the role of the water signal in the phase-sensitive voxel-wise addition of signal from each element of the multi-array external coil. In the case of water-signal unsuppressed MR spectra, the signal per coil element is high for every voxel as it is dominated by the water signal, so phasing and adding of signals from multiple elements is straightforward,[43] whereas in conventional water-suppressed MRSI, the low signal for each voxel of individual elements might cause difficulties in phasing and adding the signals from the different elements, resulting in signal loss. Although data-driven methods for coil combinations are often preferred in MR spectroscopy to mitigate this effect,[18,19] low SNR in individual coil elements inevitably influences the total signal in each voxel and it has been demonstrated for brain ^{1}H MRSI that the presence of a high residual water signal substantially improves spectroscopic SNR.[44]

The Cit maps created for the prostates of healthy volunteers show higher levels of this compound in the peripheral than the transition zone, which agrees with previous studies of healthy prostates, for which Cit tissue concentrations in the peripheral zone of up to 2–4 times higher than in the central gland were reported.[36,41]

In data from the patient with prostate cancer the increased Cho levels in the Cho concentration maps qualitatively coincided with histopathologically confirmed locations of prostate cancer. Cit concentrations varied in the peripheral zone of the prostate, with lower values not necessarily coinciding with increased choline levels. As both the T_2 and T_1 of water spins are decreased in tumor tissue the relaxation correction factor for these spins in benign and tumor tissue are similar for common TR values, implying that spatial metabolite maps directly reflect differences in their content between tumor and benign tissue.[45]

In conclusion, in this paper we present a novel procedure for efficient post-processing of water-unsuppressed MRSI of the prostate, including several steps to improve the quality of the spectroscopic data. It facilitates to exploit the advantages of water-unsuppressed MRSI, such as absolute quantification of MRS-visible metabolites instead of relying on metabolite ratios, as is common in prostate MRSI studies (e.g., Kobus et al. and Fütterer et al.)[46,47] This helps to better identify tumor tissue.[17] This novel post-processing procedure is anticipated to facilitate automation of water-unsuppressed MRSI of the prostate and to further extend its diagnostic capabilities.

ACKNOWLEDGMENTS

This project has received funding from the European Union's Horizon 2020 research and innovation program under the Marie Sklodowska-Curie grant agreement 813120. We acknowledge Siemens Healthcare for providing the MRSI sLASER WIP pulse sequence. S.v.H received funding from the Flemish Government (AI Research Program) and is affiliated with Leuven, AI-KU Leuven institute for AI, B-3000, Leuven, Belgium. We also acknowledge H.N. Bharath for providing the code of the Löwner BSS algorithm and for helpful hints.

ORCID

Angeliki Stamatelatou https://orcid.org/0000-0002-3956-8731
Arend Heerschap https://orcid.org/0000-0001-9930-4562

REFERENCES

1. Sung H, Ferlay J, Siegel RL, et al. Global cancer statistics 2020: GLOBOCAN estimates of incidence and mortality worldwide for 36 cancers in 185 countries. *CA Cancer J Clin*. 2021;71:209-249.
2. Padhani AR, Weinreb J, Rosenkrantz AB, Villeirs G, Turkbey B, Barentsz J. Prostate imaging-reporting and data system steering committee: PI-RADS v2 status update and future directions. *Eur Urol*. 2019;75:385-396.
3. Hambrock T, Somford DM, Huisman HJ, et al. Relationship between apparent diffusion coefficients at 3.0-T MR imaging and Gleason grade in peripheral zone prostate cancer. *Radiology*. 2011;259(2):453-461. doi:10.1148/radiol.091409
4. Berman RM, Brown AM, Chang SD, et al. DCE MRI of prostate cancer. *Abdom Radiol (NY)*. 2016;41:844-853.
5. Tayari N, Heerschap A, Scheenen TWJ, Kobus T. In vivo MR spectroscopic imaging of the prostate, from application to interpretation. *Anal Biochem*. 2017;529:158-170. doi:10.1016/j.ab.2017.02.001
6. Weinreb JC, Barentsz JO, Choyke PL, et al. PI-RADS prostate imaging—reporting and data system: 2015, version 2. *Eur Urol*. 2016;69:16-40.
7. Gupta RT, Mehta KA, Turkbey B, Verma S. PI-RADS: past, present, and future. *J Magn Reson Imaging*. 2020;52:33-53.
8. Turkbey B, Rosenkrantz AB, Haider MA, et al. Prostate imaging reporting and data system version 2.1: 2019 update of prostate imaging reporting and data system version 2. *Eur Urol*. 2019;76:340-351.
9. Gholizadeh N, Greer PB, Simpson J, et al. Diagnosis of transition zone prostate cancer by multiparametric MRI: added value of MR spectroscopic imaging with sLASER volume selection. *J Biomed Sci*. 2021;28:54. doi:10.1186/s12929-021-00750-6
10. Drost FJH, Osses D, Nieboer D, et al. Prostate magnetic resonance imaging, with or without magnetic resonance imaging-targeted biopsy, and systematic biopsy for detecting prostate cancer: a Cochrane systematic review and meta-analysis. *Eur Urol*. 2020;77:78-94.
11. Smith CP, Harmon SA, Barrett T, et al. Intra- and interreader reproducibility of PI-RADSv2: a multireader study. *J Magn Reson Imaging*. 2019;49:1694-1703.
12. Kobus T, Vos PC, Hambrock T, et al. Prostate cancer aggressiveness: In vivo assessment of MR spectroscopy and diffusion-weighted imaging at 3 T. *Radiology*. 2012;265:457-467.
13. Maas MC, Litjens GJS, Wright AJ, et al. A single-arm, multicenter validation study of prostate cancer localization and

aggressiveness with a quantitative multiparametric magnetic resonance imaging approach. *Invest Radiol*. 2019;54(7):437-447. doi:10.1097/RLI.0000000000000558
14. Mescher M, Tannus A, O'Neil Johnson M, Garwood M. Solvent suppression using selective echo dephasing. *J Magn Reson—Ser A*. 1996;123:226-229.
15. Dong Z. Proton MRS and MRSI of the brain without water suppression. *Prog Nucl Magn Reson Spectrosc*. 2015;86:65-79. doi:10.1016/j.pnmrs.2014.12.001
16. Serrai H, Clayton DB, Senhadji L, Zuo C, Lenkinski RE. Localized proton spectroscopy without water suppression: removal of gradient induced frequency modulations by modulus signal selection. *J Magn Reson*. 2002;154:53-59.
17. Tayari N, Wright A, Heerschap A. Absolute choline tissue concentration mapping for prostate cancer localization and characterization using 3D ^{1}H MRSI without water-signal suppression. *Magn Reson Med*. 2022;87(2):561-573.
18. Rodgers CT, Robson MD. Receive array magnetic resonance spectroscopy: whitened singular value decomposition (WSVD) gives optimal bayesian solution. *Magn Reson Med*. 2010;63:881-891.
19. Rodgers CT, Robson MD. Coil combination for receive array spectroscopy: are data-driven methods superior to methods using computed field maps? *Magn Reson Med*. 2016;75:473-487.
20. de Graaf RA. *In Vivo NMR Spectroscopy: Principles and Techniques*. John Wiley & Sons. 3rd ed.; 2019.
21. Le Fur Y, Cozzone PJ. Hemi-spectrum substitution after water signal fitting (HESWAF): an improvement of the modulus post-processing of MR spectra. *MAGMA*. 2015;28:67-85.
22. Nagaraja BH, Debals O, Sima DM, Himmelreich U, De Lathauwer L, Van Huffel S. Tensor-based method for residual water suppression in ^{1}H magnetic resonance spectroscopic imaging. *IEEE Trans Biomed Eng*. 2019;66:584-594.
23. Le Fur Y, Cozzone PJ. FID modulus: a simple and efficient technique to phase and align MR spectra. *MAGMA*. 2014;27(2):131-148. doi:10.1007/s10334-013-0381-8
24. Laudadio T, Mastronardi N, Vanhamme L, Van Hecke P, Van Huffel S. Improved Lanczos algorithms for blackbox MRS data quantitation. *J Magn Reson*. 2002;157:292-297.
25. Pijnappel WWF, van den Boogaart A, de Beer R, van Ormondt D. SVD-based quantification of magnetic resonance signals. *J Magn Reson*. 1992;97:122-134.
26. Jupin M, van Heijster FHA, Heerschap A. Metabolite interactions in prostatic fluid mimics assessed by ^{1}H NMR. *MAGMA* Published online. 2021;35:683-694.
27. Steinseifer IK, Van Asten JJA, Weiland E, Scheenen TWJ, Maas MC, Heerschap A. Improved volume selective ^{1}H MR spectroscopic imaging of the prostate with gradient offset independent adiabaticity pulses at 3 tesla. *Magn Reson Med*. 2015;74(4):915-924. doi:10.1002/mrm.25476
28. Ernst R, Bodenhausen G, Wokaun A. Principles of nuclear magnetic resonance in one and two dimensions. *Magn Reson Med*. 1988;7:253. doi:10.1002/mrm.1910070215
29. https://gitlab.esat.kuleuven.be/biomed-public/tensor-based-mrsi-gui/-/tree/edc38921ddba3c063d16041adbeef4540244d279/.
30. Poullet JB, Sima DM, Van Huffel S, Van Hecke P. Frequency-selective quantitation of short-echo time ^{1}H magnetic resonance spectra. *J Magn Reson*. 2007;186:293-304.
31. Provencher SW. Automatic quantitation of localized in vivo ^{1}H spectra with LCModel. *NMR Biomed*. 2001;14:260-264.
32. Gibbs P, Liney GP, Pickles MD, Zelhof B, Rodrigues G, Turnbull LW. Correlation of ADC and T_2 measurements with cell density in prostate cancer at 3.0 tesla. *Invest Radiol*. 2009;44:572-576.
33. de Bazelaire CMJ, Duhamel GD, Rofsky NM, Alsop DC. MR imaging relaxation times of abdominal and pelvic tissues measured in vivo at 3.0 T: preliminary results. *Radiology*. 2004;230:652-659.
34. Baur ADJ, Hansen CM, Rogasch J, et al. Evaluation of T_1 relaxation time in prostate cancer and benign prostate tissue using a modified look-locker inversion recovery sequence. *Sci Rep*. 2020;10:3121. doi:10.1038/s41598-020-59942-z
35. Ryner LN, Stroman P, Wessel T, Hoult DI, Saunders JK. Effect of oscillatory eddy currents on MR spectroscopy. *Proc 6th Annual Meeting ISMRM*, Sydney (Vol 1903). 1998.
36. Lowry M, Liney GP, Turnbull LW, Manton DJ, Blackband SJ, Horsman A. Quantification of citrate concentration in the prostate by proton magnetic resonance spectroscopy: zonal and age-related differences. *Magn Reson Med*. 1996;36:352-358. doi:10.1002/mrm.1910360305
37. Hamilton EI. Report of the task group on reference man, international commission on radiological protection publication 23. *Sci Total Environ*. 1976;6:201-202.
38. Scheenen TWJ, Klomp DWJ, Röll SA, Fütterer JJ, Barentsz JO, Heerschap A. Fast acquisition-weighted three-dimensional proton MR spectroscopic imaging of the human prostate. *Magn Reson Med*. 2004;52:80-88.
39. Dong Z, Dreher W, Leibfritz D. Toward quantitative short-echo-time in vivo proton MR spectroscopy without water suppression. *Magn Reson Med*. 2006;55:1441-1446.
40. Cabanes E, Confort-Gouny S, Le Fur Y, Simond G, Cozzone PJ. Optimization of residual water signal removal by HLSVD on simulated short echo time proton MR spectra of the human brain. *J Magn Reson*. 2001;150:116-125.
41. Basharat M, Jafar M, de Souza NM, Payne GS. Evaluation of short-TE ^{1}H MRSI for quantification of metabolites in the prostate. *NMR Biomed*. 2014;27(4):459-467. doi:10.1002/nbm.3082
42. De Graaf AA, van Dijk JE, BoéE WMMJ. Quality: quantification improvement by converting lineshapes to the lorentzian type. *Magn Reson Med*. 1990;13:343-357.
43. Brown MA. Time-domain combination of MR spectroscopy data acquired using phased-array coils. *Magn Reson Med*. 2004;52:1207-1213.
44. Vareth M, Lupo J, Larson P, Nelson S. A comparison of coil combination strategies in 3D multi-channel MRSI reconstruction for patients with brain tumors. *NMR Biomed*. 2018;31:e3929. doi:10.1002/nbm.3929
45. Stamatelatou A, Scheenen TWJ, Heerschap A. Developments in proton MR spectroscopic imaging of prostate cancer. *MAGMA* Published online. 2022;35:645-665.
46. Kobus T, Wright AJ, Weiland E, Heerschap A, Scheenen TWJ. Metabolite ratios in ^{1}H MR spectroscopic imaging of the prostate. *Magn Reson Med*. 2015;73:1-12.
47. Fütterer JJ, Scheenen TWJ, Heijmink SWTPJ, et al. Standardized threshold approach using three-dimensional proton magnetic resonance spectroscopic imaging in prostate cancer localization of the entire prostate. *Invest Radiol*. 2007;42:116-122.

SUPPORTING INFORMATION

Additional supporting information may be found in the online version of the article at the publisher's website.

Figure S1. Removing sidebands in the spectral region of the metabolites of interest.(A) Water sidebands around 6.1 and 3.3 ppm in an in vivo MR spectrum from a healthy volunteer. The sideband artifacts are symmetrically present on both sides of the water peak in the raw signal, interfering with the region of the metabolites of interest (box from 2.3–3.6 ppm).(B) Spectral shape before sideband removal, with k-space Hamming filter. (C) Spectral shape before sideband removal, without k-space Hamming filter. (D) Spectral shape after the modulus operation, without k-space Hamming filter. (E) Spectral shape after the modulus operation and Hilbert transformation, without k-space Hamming filter. (F) Spectral shape after the modulus operation, Hilbert transformation and k-space Hamming filter. The spectra in b and f originate from the same voxel size (both Hamming-filtered) and can be compared to assess the effect of the sideband removal.

Figure S2. LCModel reports of a voxel in the phantom solution. (A) Spectrum from water-signal unsuppressed MRSI with water signal removal in post-processing using Löwner BSS. (B) Spectrum from water signal suppressed MRSI. Note the deviating citrate shape because of the different interpulse timing of the sequence used here (TE 88 ms, alternative inter-pulse timing)

Figure S3. LCModel report of a voxel in healthy prostate tissue.

Figure S4. LCModel report of a spectrum of a voxel within cancer tissue.

How to cite this article: Stamatelatou A, Sima DM, van Huffel S, van Asten JJA, Heerschap A, Scheenen TWJ. Post-acquisition water-signal removal in 3D water-unsuppressed ^{1}H-MR spectroscopic imaging of the prostate. *Magn Reson Med*. 2023;89:1741-1753. doi: 10.1002/mrm.29565